JAAS

PAPER

View Article Online
View Journal | View Issue

Cite this: J. Anal. At. Spectrom., 2023, 38, 1224

An optimization method based on spatial confinement for direct detection of laser-induced particle flow

Hongjie Chen,[ab] Meirong Dong, †*[ab] Junbin Cai,[ab] Zihan Shang,[ab] Zhichun Li,[ab] Feiqiang Tang[ab] and Jidong Lu [ab]

Laser-induced breakdown spectroscopy (LIBS) has the advantages of on-line, rapid and multi-element synchronous detection. It can be applied to real-time and rapid property detection of particle flow. However, the instability of flow greatly affects the quality and stability of laser–material interaction and plasma generation. Therefore, to improve the stability of interaction, a section of a perforated hollow quartz tube was developed and attached to the laser ablation position of particle flow to form a cylindrical spatial confinement for the particle flow and its plasma. The confinement and stabilization effects of the cylindrical spatial confinement were investigated by using plasma images, pulse-to-pulse relative standard deviation (RSD) images and statistical analysis of spectral data. In addition, the effects of the cylindrical spatial confinement in different particle flow scenarios were compared to explore the impact of particle size on the application. The results showed that the cylindrical spatial confinement is effective in confining the particle flow and plasma, but the confinement effect is particle size dependent and the difference would be directly reflected in the improvement amplitude of the signal-to-noise ratio (SNR). In addition, the analysis of pulse-to-pulse RSD images of the plasma and the pulse-to-pulse RSDs of the characteristic emissions showed that the cylindrical spatial confinement can effectively improve the stability of LIBS particle flow detection, and the particle size has no obvious impact on the stability effect of spatial confinement. In general, cylindrical spatial confinement can effectively confine and stabilize the plasma of the particle flow, thus improving the quality of the particle flow spectral signal.

Received 5th February 2023
Accepted 18th April 2023

DOI: 10.1039/d3ja00041a

rsc.li/jaas

1. Introduction

Laser-induced breakdown spectroscopy (LIBS) is an atomic emission spectroscopy technique characterized by rapid detection, real time, minor damage, and simultaneous analysis of multiple elements and does not require a complex sample preparation process.[1–3] LIBS is considered widely suitable for the analysis of solids, liquids and gases.[4] Online analysis of particle flow is necessary in many fields of industrial manufacturing, such as monitoring of pulverized coal quality, detection of unburned carbon of fly ash, additive manufacturing of metal parts, and detection of cement raw materials.[5–7] Therefore, more and more researchers have begun to employ LIBS to analyze gas–solid two-phase flow directly.[8–10] One of the obvious advantages of LIBS detection on particles in particle flow is the absence of complex sample preparation and the simplicity of the detection device.[5] It significantly reduces the cycle time for testing and better characterizes the material in its industrial process state. However, there are many factors that affect the stability of analysis when LIBS is used to obtain spectral data by direct ablation of the particle flow, resulting in weak signal intensity, poor representativeness and low repeatability of the acquired spectral message. For example, there is an inevitable fluctuation in the particle flow that affects the quality and stability of the laser–particle coupling. The particle size of the sample also has an important impact on the particle concentration in the ablation zone, resulting in fluctuations in particle ablation quality and differences in plasma location and evolution.[11] At the same time, part of the laser energy is absorbed by the particles deviating the laser focal point and by the gaseous medium between the particles in the ablation zone, and also interacts with the existing plasma and accompanied shockwaves. This will lead to more irregular plasma shapes like the formation of two or more plasma cores.[12] Combined with the fluctuating nature of the laser energy, the spectral signal may show large variations.[13] This causes plasma generated in particle flow often exhibiting greater fluctuations in their size, shape and position compared to plasma generated on solid

[a]School of Electric Power, South China University of Technology, Guangzhou, Guangdong, 510640, China. E-mail: epdongmr@scut.edu.cn; jdlu@scut.edu.cn

[b]Guangdong Province Engineering Research Center of High Efficient and Low Pollution, Guangzhou, Guangdong, 510640, China

† Present address: No. 381 Wushan Road, Tianhe District, School of Electric Power, South China University of Technology, Guangzhou, Guangdong, 510640, China.

surfaces, resulting in greater signal instability.[2] The poor intensity and repeatability of the spectral signal are finally reflected in the analysis performance.

Therefore, many improvement methods have been proposed for these negative impacts, which can be divided into two categories. One category focuses on the spectral data and uses mathematical methods to select or correct the spectral data to improve the reliability of LIBS detection. The other category focuses on the experimental system and uses physical methods to improve the intensity and repeatability of the LIBS signal of particle flow. In terms of mathematical methods, a series of spectral pre-processing methods have been proposed such as: spectral line intensity normalization,[14] internal standard method,[15] sieve and removal invalid spectra,[16] and other methods.[17] Actually, it is important to optimize the experimental system to improve the particle flow detection by LIBS. Some researchers adopted the method of sampling particle samples before detection to avoid the detection instability caused by the fluctuation of particle flow. Yin and Zhang *et al.*[18] proposed an online detection method that collected pulverized coal into a container to form a static surface for laser ablation detection. The results show that the relative error of the quantitative analysis of the elements is all less than 10%. Zhan *et al.*[19] developed a coal sample preparation device based on a physical constraint for preparing pulverized coal quickly, which can quickly compress pulverized coal into coal pillars for laser ablation. The quantitative analysis of ash and volatile matter content was comparable to conventional coal pellet detection. Generally, this method requires relatively complex sampling devices, which may increase the complexity and cost of the detection system. Consequentially, some studies have committed to investigating optimization methods for direct particle flow detection. Yao *et al.*[20] designed a series of tapered tubes to stabilize the flow of particles and concluded that a tapered tube with an outlet orifice internal diameter of 5.5 mm was most suitable for direct analysis of pulverized coal particle flow. Yu *et al.*[21] used a metallic target to stabilize the focus position of a laser pulse on silica particle flow, and the results showed that the signal strength and signal stability of LIBS detection of particle flow could be improved. They also tried to use a double lens to improve the signal repeatability.[22] The double lens had a smaller spherical aberration that created a smaller focusing area, thus improving the signal repeatability. Liu *et al.*[23] used a short nanosecond pulse width laser to improve the reliability of fly ash particle flow detection.

The above methods are aimed at reducing or avoiding the instability of particle flow to improve the stability and strength of LIBS detection signals. Actually, there are some other methods that are widely used in many scenarios due to their simplicity and adaptability, and their effectiveness in improving the stability and strength of the LIBS detection signal. Spatial confinement is a method with these characteristics. The spatial confinement scheme restricts the expansion of plasma by adding physical barriers. Specifically, the barrier reflects the shockwave generated by the plasma to reheat the plasma and to adjust the position of the expanding plasma, so as to improve the spectral intensity and the signal repeatability.[24] Popov *et al.*[25] used cylindrical spatial confinement to increase the limit of detection of different elements by a factor of 2–5. Moreover, the parts used to achieve spatial confinement can also be designed according to the actual scene. Yin *et al.*[26] designed a bowl-shaped spatial confinement in conjunction with the air plasma shape, which was able to reduce the pulse-to-pulse RSDs from 11.96% and 12.25% to 2.97% and 3.94% for N $I_{742.36}$ (one of the characteristic spectral lines of nitrogen) and O $I_{777.42}$ (one of the characteristic spectral lines of oxygen), respectively. The spatial confinement is also convenient to cooperate with other optimization methods to make the enhancement effect more significant because of its simplicity and compatibility. Guo *et al.*[27] combined dual-pulse LIBS (DP-LIBS) with spatial confinement to enhance the enhancement factor for the emission intensity of chromium (Cr) lines from 106.1 (only DP-LIBS) to 168.8 (combining spatial confinement and dual-pulse). They also used a combination of spatial and magnetic confinement to enhance laser-induced plasma light emission and indicated that the enhancement effect of using both together was much stronger than that of using only spatial confinement.[28] The spatial confinement is also effective in femtosecond laser-induced breakdown spectroscopy (fs-LIBS) detection. Zhao *et al.*[29] investigated the spatial confinement effect on Pb measurements in soil by fs-LIBS. The results showed that the spatial confinement can improve the detection sensitivity and the detection accuracy of fs-LIBS. Some studies have shown that spatial confinement can improve the strength and repeatability of LIBS detection signals,[25–29] and it has the advantage of simple equipment, low cost and strong adaptability. Therefore, in this work, we tried to apply spatial confinement to the detection of particle flow by LIBS. A modified cylindrical spatial confinement was designed based on the characteristics of the particle flow. Then the plasma images and the performance of spectral data before and after adding confinement were compared and analyzed. In addition, considering the influence of the matrix effect caused by different particle sizes, the influence of the particle size on the effect of cylindrical space confinement was also explored.

2. Experimental

The experimental system in this work includes a LIBS setup, particle flow device and cylindrical spatial confinement

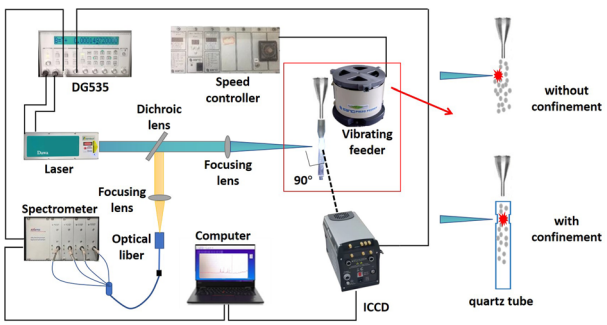

Fig. 1 Schematic diagram of the experimental setup.

settings, as shown in Fig. 1. Silica particles were selected as the experimental samples. A piezoelectric vibrating feeder (PEF-90A, Sanki, Japan) can drop the experimental samples into the pipe by a vibrating screen to form a particle flow with a diameter of 4 mm. A speed control module was used to control the speed of the silica particle flow, controlling the feeder vibration frequency and maintaining an average mass flow rate of 1.3 ± 0.05 g min^{-1} for the silica particle flow. In the system, a Q-switched Nd:YAG laser (Dawa-200, Beamtech, China) was employed as the laser source, with a wavelength of 1064 nm and a pulse width of 8 ns. The laser pulse repetition rate was set at 2 Hz to reduce the mutual interference between different pulses. In this experiment, a focusing lens with a diameter of 25.4 mm and a focal length of 100 mm was selected to focus the laser pulse to the center of the particle flow beam. The plasma light was reflected by a 45° long pass dichroic mirror (reflection band 200–785 mm and transmission band 825–1300 nm), and then focused into the optical fiber probe through the focusing lens. After the signal was collected by an optical fiber, and the system used a four-channel optical fiber spectrometer (Netherlands Avantes, AvaSpec-2048) for detection with a gate width of 1.05 ms, covering a spectral range from 178 to 827 nm with a nominal resolution of about 0.1 nm. For the plasma morphology, an ICCD camera (Andor, iStar 334T) was used in the system to capture images from a vertical angle to the laser beam. The system used a digital delay generator (DG535, Stanford Research System, USA) to associate the ICCD camera, spectrometer and laser, so as to achieve the synchronization of laser output, spectrum and image acquisition. After parameter experiment optimization, this experiment set the delay time from the laser output trigger signal to spectrometer scanning as 1 μs, and the laser energy as 90 mJ to obtain the best signal-to-noise ratio (SNR). Meanwhile, the gate width and delay time (the time from the laser output trigger signal to the start of ICCD shooting) of the ICCD were set to 0.1 μs and 1 μs respectively.

Based on the flow and excitation characteristics of particle flow, a hollow quartz tube with an outer diameter of 6 mm and an inner diameter of 4 mm was developed to form the cylindrical spatial confinement. To avoid laser ablation on the pipe wall, two slits were symmetrically created on the pipe wall. In this way, the laser can directly ablate the particle flow and the quartz tube will not affect the incidence and propagation of the laser.

To explore the influence of particle size on the confinement effect, silica particles with four particle size types that are commonly used in industry were employed, as shown in Table 1. All four particle size types were sieved through the sieve. For example, samples in the particle size range 125–200 μm were able to pass through the 200 μm pore size sieve but not the 125 μm sieve. Under each experimental condition and specimen, the particle flow was ablated 600 times continuously by a laser while collecting spectral data and plasma images for subsequent analysis.

Table 1 The particle size distribution of silica samples

Sample no.	Sample name	Particle size range (μm)
1	Silicon dioxide	200–250
2		125–200
3		80–125
4		58–75

3. Results and discussion

3.1 Investigation on the effectiveness of cylindrical spatial confinement based on ICCD plasma images

Studies have pointed out that the plasma dynamics can be more effectively studied and analysed by observing the plasma morphology.[30] Therefore, the plasma images of silica particles of different particle size ranges with and without cylindrical spatial confinement were compared to preliminarily verify the effectiveness of the cylindrical spatial confinement in confining the plasma of particle flow. The 600 pulsed plasma images obtained in each case were averaged and plotted using the same colour bars to obtain the plasma images in each of the following cases. The pixel points of each image within this subsection were normalized by using eqn (1):

$$X'_{\text{pixel}} = \frac{X_{\text{pixel}} - \min(X_{\text{pixel}})}{\max(X_{\text{pixel}}) - \min(X_{\text{pixel}})} \quad (1)$$

where X'_{pixel} represents the normalized pixel value, and X_{pixel} represents the pixel value in the original data. The max means to round the maximum value of the original pixel in the following eight images up to the nearest integer, and the min means to round the minimum value down to the nearest integer.

In the plasma image, the flow direction of the particles is vertical downward, and the incident direction of the laser is horizontal to the right at the position of about 5.5 mm at the *Y*-axis. The abscissa of the laser's focus position is approximately 4 mm on the *X*-axis. Fig. 2 shows the plasma morphology of

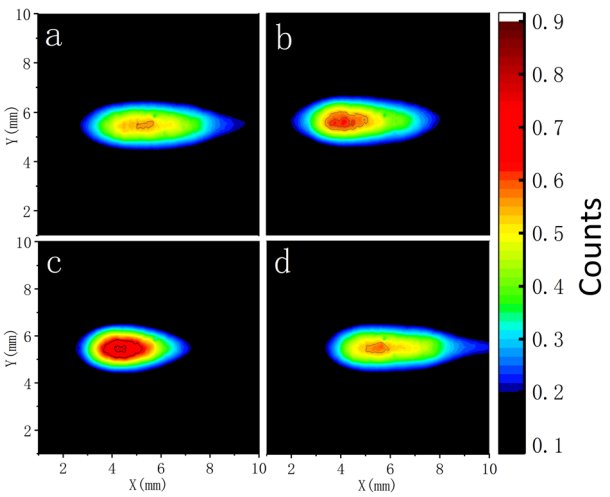

Fig. 2 Plasma averaged count images taken by the ICCD without cylindrical spatial confinement at a particle size of (a) 200–250 μm, (b) 125–200 μm, (c) 80–125 μm, and (d) 58–75 μm.

silica particles of four particle size types in the absence of spatial confinement. All images are collected under the same ICCD parameter settings (the same delay time and gate time), and the normalization of pixel values is processed under the same standard. Therefore, the following images can be compared with gray values to discuss the plasma emission and compare the brightness. From the image display, it can be seen that the plasma is elliptical in shape. The axial length of the plasma backward along the laser incidence direction is longer, so it can be judged that the expansion speed of the plasma backward along the laser pulse propagation direction is faster. This phenomenon is due to the laser-supported detonation wave (LSD). The expanding plasma absorbs energy from the tail of the laser pulse, leading to a preferential expansion of the shockwave along the axial direction of the laser pulse.[31,32] However, there are some differences in the plasma morphology at different particle sizes. Silica particles with a particle size range of 80–125 μm show the brightest brightness of the plasma center among the four particle size types, and the plasma center shows a large area of high brightness values. From the abscissa of the plasma center, it can be observed that there are certain differences in the plasma positions of different particle sizes. It may be that the difference of particle size affects the position of laser-excited particle samples, resulting in a shift in the position of the plasma at the same focal point setting. This phenomenon reflects the unstable characteristics of LIBS breakdown particle flow. Moreover, it can be seen that compared with the plasma of 80–125 μm silica particles, the area of silica plasma of the other three particle sizes is larger. This indicates that the other three plasmas may have larger initial plasma size and are probably quenched earlier in comparison.

The images of the silica plasma with the four particle size types with the cylindrical spatial confinement are shown in Fig. 3. It is obvious that plasma with different particle sizes is subject to different degrees of confinement. The compressed shape displayed is also different. For silica particles with particle size ranges of 80–125 μm and 58–75 μm, the plasma center brightness is significantly stronger than that without confinement. It means that the radiation intensity of the plasma center has been significantly improved. As the accompanying shockwave is confined by the pipe wall and interferes with the plasma after reflection, the plasma shows an undulation and compression state. This reflected shockwave can not only adjust the shape of the plasma, but also reheat it. For plasma with silica particles in the particle size range of 200–250 μm and 125–200 μm, the plasma shape also changed. The center of the plasma appears to be compressed, but the plasma as a whole does not seem to be significantly compressed like the plasma with silica particles in the particle size ranges of 80–125 μm and 58–75 μm. There is not very significant increase in the plasma center brightness, and the head and tail of the plasma show a long strip state of being squeezed due to expansion towards the outside of the pipe slit. These phenomena show that cylindrical spatial confinement can indeed achieve the effect of confining the plasma, but the degree of confinement has a certain relationship with the particle size.

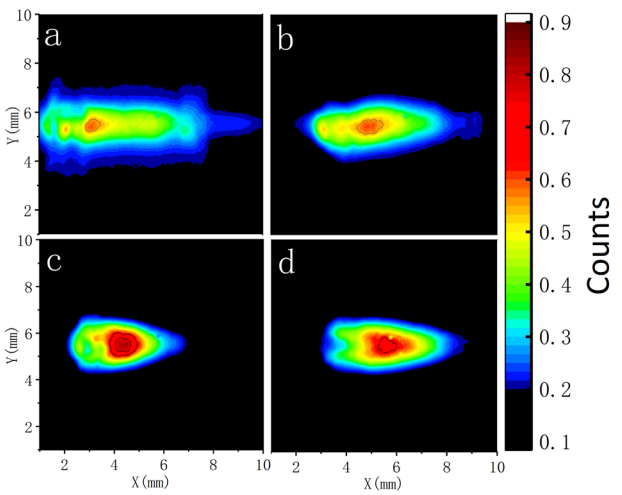

Fig. 3 Plasma averaged count images taken by the ICCD with cylindrical spatial confinement at a particle size of (a) 200–250 μm, (b) 125–200 μm, (c) 80–125 μm, and (d) 58–75 μm.

3.2 Verification of stabilization by pulse-to-pulse RSD images of plasma

The pulse-to-pulse RSD images of plasma were recorded and plotted to explore the effect of adding spatial confinement on the enhancement of the stability of the direct detection of particle flow by LIBS. The pulse-to-pulse RSD images were plotted from a pixel-by-pixel calculation of a pulse-by-pulse plasma image, and the sample size remained the same at 600 pulses per case. Take a pixel as an example, and the calculation formula is shown in eqn (2):

$$\mathrm{RSD}_{\mathrm{pixel}} = \frac{1}{X_{\mathrm{ave}}}\sqrt{\frac{\sum_{i=1}^{n}\left(X_{i\mathrm{pixel}} - X_{\mathrm{ave}}\right)^2}{n-1}} \quad (2)$$

where X_{ave} is the average of the total number of images (n) for that pixel, and $X_{i\mathrm{pixel}}$ is the pixel value in the i^{th} image of the total number of images (n). In this case, n is 600. The $\mathrm{RSD}_{\mathrm{pixel}}$ of all pixels was calculated and the pulse-to-pulse RSD images of plasma can be obtained as shown in Fig. 4. And the same color bar was used in each case in Fig. 4.

As shown in Fig. 4, the RSD values show up as being larger at both ends of the plasma and smaller in the middle without adding spatial confinement. This situation shows a relatively low RSD in the core region of the plasma, but large fluctuations in the anterior and posterior parts of plasma along the laser incidence direction, which are mainly related to changes in the position of the plasma, indicating that there is either a forward or posterior shift in the breakdown position. This is also related to the generation and expansion process of plasma. The morphology of the pulse-to-pulse RSD images is approximately the same between the different particle sizes, but there are significant differences in RSDs. This reflects the instability of the particle flow plasma and the effect of particle size on the signal stability.

After the addition of the cylindrical spatial confinement, it can be seen that the RSD decreases for all four particle size types

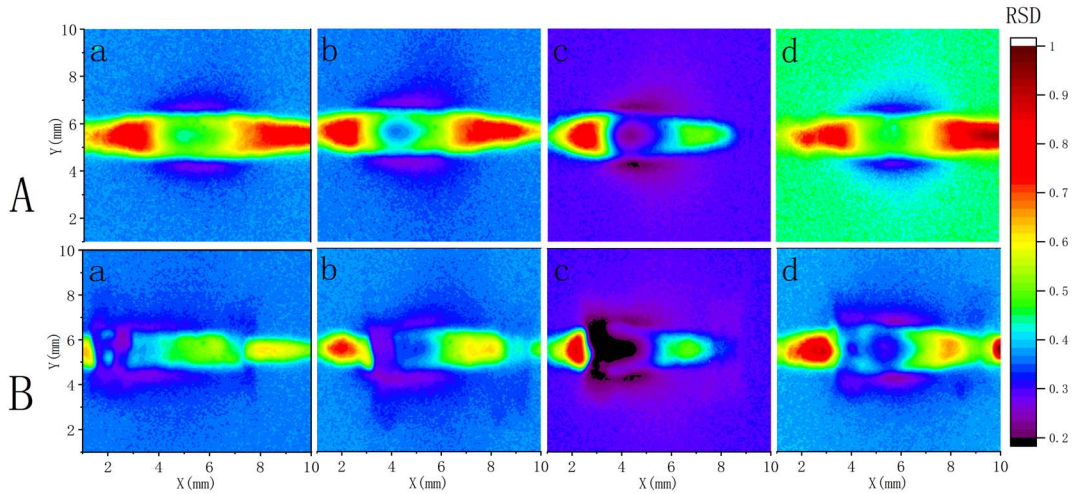

Fig. 4 Pulse-to-pulse RSD images of plasma taken by the ICCD (A) without cylindrical spatial confinement, and (B) with cylindrical spatial confinement, at a particle size of (a) 200–250 μm, (b) 125–200 μm, (c) 80–125 μm, and (d) 58–75 μm.

and the stabilization effect is mainly concentrated in the plasma core region. This reflects the more stable focal position of the laser-ablated particles, indirectly indicating that cylindrical spatial confinement reduces the impact of unstable particle flow on LIBS detection. The plasma emission mainly comes from the plasma core, and the stability of the core is beneficial to the acquisition of spectral data.[33] Combined with the confinement effect and stabilization effect of the cylindrical spatial confinement on the plasma, indicating that the method improves the reliability of the particle flow signal detected by LIBS. In addition, the influence of particle size on the effect of spatially constrained stable plasma of particle flow cannot be clearly seen from the image comparison between different particle sizes. The stabilization effect is relatively effective as a whole.

3.3 Investigation on the effectiveness of cylindrical spatial confinement based on spectral data

Statistical analysis of the spectral data has been carried out, to further confirm and analyze the effect of cylindrical spatial confinement on the compression and stabilization of the plasma. The differences manifested when spatial confinement was applied to different particle sizes were also analyzed. In the process of LIBS particle flow detection, the ablation effect and stability will be greatly affected due to the particle flow fluctuations and other reasons. When conditions such as small effective ablation masses or large fluctuations in the plasma position occur, the resulting plasma spectra cannot effectively characterize the particle composition information. The phenomenon presented is that the spectrum does not contain the excitation characteristic lines of the main elements or even only contains the excitation characteristic lines of the main elements with weak intensity, which is generally regarded as an invalid spectrum. The main reason is that the fluctuation of particle flow causes the position of the laser breakdown particle sample to deviate from the focus and the fluctuation of sample mass in the laser ablation zone. The fluctuation of the particle sample mass in the laser ablation zone would cause the change of the fraction of the gaseous medium (air) in the zone. When the mass of the particle sample in the ablation zone decreases, the air proportion increases, resulting in a decrease in the effective ablation mass and an increase in the proportion of laser-excited air. This would lead to the increase in the intensity of the characteristic spectral lines of the elements in the air (such as N), and a decrease in the intensity of the characteristic spectral lines of the elements in the sample (such as Si). Therefore, to reflect that the addition of spatial confinement can reduce the fraction of the gaseous medium (air) in the ablation zone and improve the absorption of laser energy by particle samples from the spectral data, the parameter air breakdown ratio β was introduced.[21] Since the sample basically contains no nitrogen element, the parameter is chosen as the ratio of the peak intensity of the spectral line of nitrogen ($I_{\mathrm{N\ I746.83}}$) to the peak intensity of the spectral line of silicon ($I_{\mathrm{Si\ I288.16}}$). Eqn (3) is as follows:

$$\beta = \frac{I_{\mathrm{N\ I746.83}}}{I_{\mathrm{Si\ I288.16}}} \tag{3}$$

The changes of the spectral SNRs and air breakdown ratio after adding spatial confinement were also analyzed for the purpose of verifying the improvement of effective breakdown brought about by the plasma which is confined and stabilized by spatial confinement. The calculation formula of the SNR is shown in eqn (4):

$$\mathrm{SNR} = \frac{I - \mathrm{avg}}{\mathrm{SD}} \tag{4}$$

where I is the signal strength, avg is the average value of the surrounding background value of the observed spectral line, and SD is the standard deviation of the background spectral line intensity.

Two characteristic spectral lines of silicon (Si $I_{251.61}$ nm and Si $I_{288.16}$ nm) and one characteristic spectral line of nitrogen (N $I_{746.83}$ nm) are chosen for analysis. Fig. 5 shows the comparison

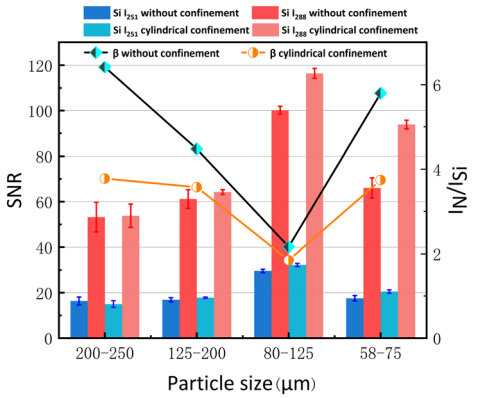

Fig. 5 SNRs of Si $I_{251.61}$ and Si $I_{288.16}$ with and without cylindrical spatial confinement at different particle sizes.

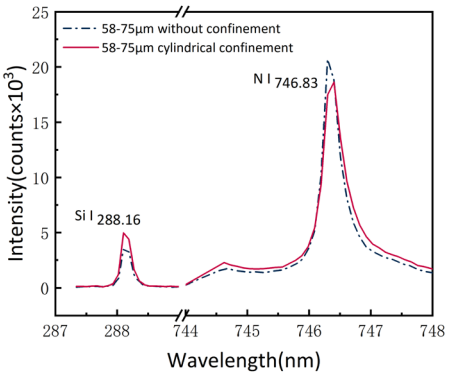

Fig. 6 Spectra comparison of Si $I_{288.16}$ and N $I_{746.83}$ with and without cylindrical spatial confinement at a particle size of 58–75 μm.

of the 600 pulse average SNR of Si $I_{251.61}$ and Si $I_{288.16}$ of silica particles with different particle sizes and their air breakdown ratio before and after adding spatial confinement. The error bar was obtained by dividing 600 pulses into five groups on average and calculating the standard deviation between groups. As can be seen in Fig. 5, the improvement effect of spatial confinement on SNRs is indeed affected by particle size, and the improvement effect of the two particle types with smaller particle size is more obvious. The silicon spectral SNRs of 80–125 μm silica particles are increased from 29.62 and 100.20 to 32.28 and 116.40 respectively. The SNRs of the silicon spectrum of 58–75 μm silicon dioxide particles increase from 17.58 and 66.05 to 20.55 and 93.88, respectively. This is exactly in line with the phenomena exhibited by the plasma when it is confined. It directly reflects the improvement effect of cylindrical spatial confinement on the SNR and effective breakdown of LIBS detection particle flow.

Combining the above studies, the occurrence of this particle discrepancy phenomenon should be related to the stability of the silica particle flow, the homogeneity of the particles and the density of the particles in the ablation zone. Differences in the particle density and air gap rate in the ablation zone can cause differences in laser ablation, the stability of the plasma morphology, brightness and position, ultimately manifesting themselves in different effects after the addition of spatial confinement. Non-ideal effects such as aerodynamic lift on particles during the forming and expansion process of particle flow will lead to broadening of particle beams.[34] Therefore, measurement with spatial confinement can ablate to a more compact particle beam, which facilitates the ablation of the sample by the laser and increases effective breakdown. Particles with larger particle size are more likely to collide with the constrained surface and with each other because of inertial effects. Such collisions will cause more rotation, resulting in abrupt changes in particle trajectories and velocities.[35] Therefore, the flow of the two particle types with larger particle size under the spatial confinement is more unstable than that of the particles with smaller particle size. As can be seen from the plasma image and the parameter β, the plasma position is more unstable and the proportion of air excited by the laser is larger for the two particle types with larger particle sizes. This results in a poor ablation effect and affects the effect of spatial confinement causing an inconspicuous SNR improvement. In contrast, the two particle types with smaller particle sizes can achieve a better confinement effect by adding spatial confinement on the basis of the favorable ablation effect, and fluctuations in the particle flow can be stabilized more significantly for the two smaller particle size types with the addition of confinement, resulting in better improvement in the SNR.

Fig. 5 also shows that the air breakdown ratio decreases for all four particle size types after the addition of confinement, indicating that spatial confinement reduces the absorption of laser energy by the gaseous medium (air) and increases the effective breakdown of particles by the laser. Furthermore, the 58–75 μm silica particles were taken as an example to analyse the changes of the spectra after adding confinement. The 600 pulses before and after the addition of the confinement were averaged separately and the characteristic spectral lines of Si $I_{288.16}$ (band 287–290 nm) and N $I_{746.83}$ (band 744–748 nm) were intercepted to draw Fig. 6. As can be seen, after adding the confinement, the strength of Si $I_{288.16}$ becomes stronger, and the corresponding strength of N $I_{746.83}$ becomes weaker. It is confirmed that the addition of cylindrical spatial confinement improved the absorption of laser energy by the sample particles to achieve more effective breakdown.

Finally, the stabilization effect of cylindrical spatial confinement on the detection of particle flow by LIBS was verified by comparing the pulse-to-pulse RSDs of Si $I_{251.61}$ before and after the confinement. Furthermore, we compare the RSDs of Si $I_{251.61}$ before and after the elimination of invalid spectra in each case. In this experiment, invalid spectra were eliminate using the standard deviation (SD) method.[8] Taking Si $I_{288.16}$ as the selected feature peak, the standard deviation of the intensity of 5 pixels in its emission line profile was calculated. All spectra with an SD of less than 94 were considered invalid.[21] The pulse-to-pulse RSDs of Si $I_{251.61}$ were calculated for each case in the four particle size ranges to obtain Fig. 7. The calculation method of RSD is equivalent to eqn (2), where the pixel value was replaced by the characteristic peak value. It can be found that this confinement leads to a more effective stabilization

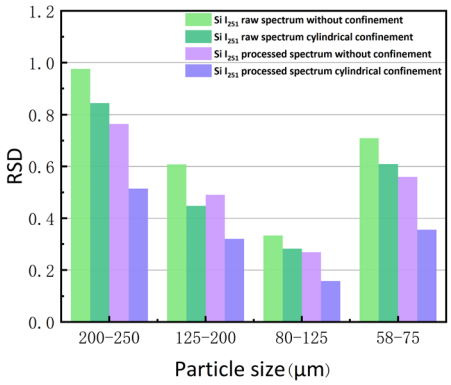

Fig. 7 Pulse-to-pulse RSDs of Si $I_{251.61}$ of raw and processed spectra with and without cylindrical spatial confinement at different particle sizes.

effect. For silica particles with four particle size types, the addition of cylindrical spatial confinement improves the signal repeatability of Si $I_{251.61}$ in the case of analyzing raw data. The pulse-to-pulse RSDs of Si $I_{251.61}$ of the 200–250 μm and 58–75 μm silica particles are reduced from 0.975 and 0.709 to 0.844 and 0.608 respectively. The stabilization effect of adding confinement after removing invalid spectra is obvious. The pulse-to-pulse RSDs of Si $I_{251.61}$ of the 200–250 μm and 58–75 μm silica particles are reduced from 0.764 and 0.560 to 0.513 and 0.355 respectively, and the RSD of the 80–125 μm silica particles is reduced to 0.157 with confinement. The results embodied in Fig. 7 are also consistent with the results of the analysis of the pulse-to-pulse RSD images described above. The cylindrical spatial confinement stabilizes the position of the plasma, thus effectively improving the repeatability of the spectral signal. In terms of repeatability, there is no significant effect of particle size on the stabilizing effect of cylindrical spatial confinement. In summary, the addition of cylindrical spatial confinement can be effective in making the spectral signal more stable.

4. Conclusions

The accuracy and stability of LIBS detection for particle flow are inevitably affected by the instability of particle flow. In this work, a cylindrical spatial confinement was designed for improving the direct detection of particle flow by LIBS. Firstly, the effect of spatial confinement on the plasma of particle flow is verified by comparing and analyzing the plasma images before and after the addition of spatial confinement. It is also found that when applying cylindrical spatial confinement to the particle flow scenario, the confinement effect of spatial confinement on the plasma has a certain relationship with the particle size. Then the investigation on the pulse-to-pulse RSD images of plasma exhibits the improvement of plasma stability by spatial confinement. Finally, according to the statistical analysis of spectral data, the cylindrical spatial confinement can effectively improve the effective breakdown by reducing undesired gas excitation and can stabilize the signal. In general, the spatial confinement can effectively confine the plasma, stabilize the position of plasma, and improve the reliability of spectral data. Cylindrical spatial confinement has application feasibility and prospects in optimizing the quantitative analysis of LIBS particle flow.

Conflicts of interest

There are no conflicts to declare.

Acknowledgements

This work was supported by the National Natural Science Foundation of China (No. 51976064), the Guangdong Basic and Applied Basic Research Foundation (2022A1515010709), and the Fundamental Research Funds for the Central Universities (2022ZFJH004). We also acknowledge the support from the Guangdong Province Key Laboratory of Efficient and Clean Energy Utilization (2013A061401005).

References

1 M. Gaft, E. Dvir, H. Modiano and U. Schone, Laser Induced Breakdown Spectroscopy Machine for Online Ash Analyses in Coal, *Spectrochim. Acta, Part B*, 2008, **63**, 1177–1182.
2 S. Yao, J. Zhao, J. Xu, Z. Lu and J. Lu, Optimizing the binder percentage to reduce matrix effects for the LIBS analysis of carbon in coal, *J. Anal. At. Spectrom.*, 2017, **32**, 766–772.
3 X. Cheng, X. Yang, Z. Zhu, L. Guo, X. Li, Y. Lu and X. Zeng, On-stream analysis of iron ore slurry using laser-induced breakdown spectroscopy, *Appl. Opt.*, 2017, **56**, 9144–9149.
4 Z. Wang, T. Yuan, Z. Hou, W. D. Zhou, J. D. Lu, H. B. Ding and X. Y. Zeng, Laser-induced breakdown spectroscopy in China, *Front. Phys.*, 2014, **9**, 419–438.
5 J. Zheng, J. Lu, B. Zhang, M. Dong, S. Yao, W. Lu and X. Dong, Experimental study of laser-induced breakdown spectroscopy (LIBS) for direct analysis of coal particle flow, *Appl. Spectrosc.*, 2014, **68**, 672–679.
6 A. Mansoori, B. Roshanzadeh, M. Khalaji and S. H. Tavassoli, Quantitative analysis of cement powder by laser induced breakdown spectroscopy, *Opt. Lasers Eng.*, 2011, **49**, 318–323.
7 P. A. Sdvizhenskii, V. N. Lednev, R. D. Asyutin, M. Y. Grishin, R. S. Tretyakov and S. M. Pershin, Online laser-induced breakdown spectroscopy for metal-particle powder flow analysis during additive manufacturing, *J. Anal. At. Spectrom.*, 2020, **35**, 246–253.
8 S. Yao, L. Zhang, K. Ying, K. Bai, J. Xu, Z. Lu and J. Lu, Identifying laser-induced plasma emission spectra of particles in gas-solid flow based on the standard deviation of intensity across an emission line, *J. Anal. At. Spectrom.*, 2018, **33**, 1676–1682.
9 S. H. Lee and J. J. Yoh, Detection of Carbon Particulates from a High-Speed Stream Reaching 70 Meters/Second, *Appl. Spectrosc.*, 2012, **66**, 107–113.
10 R. Yoshiie, Y. Yamamoto, S. Uemiya, S. Kambara and H. Moritomi, Simple and rapid analysis of heavy metals in

sub-micron particulates in flue gas, *Powder Technol.*, 2008, **180**, 135–139.
11 S. Yao, J. Lu and Z. Lu, Influence of sample morphology on laser ablation properties of coal, *Acta Opt. Sin.*, 2009, **29**, 1126–1130.
12 C. Leela, S. Bagchi, V. R. Kumar, S. P. Tewari and P. P. Kiran, Dynamics of laser induced micro-shock waves and hot core plasma in quiescent air, *Laser Part. Beams*, 2013, **31**, 263–272.
13 J. Li, J. Lu, Z. Lin, S. Gong, C. Xie, L. Chang and P. Li, Effects of experimental parameters on elemental analysis of coal by laser-induced breakdown spectroscopy, *Opt. Laser Technol.*, 2009, **41**, 907–913.
14 M. Dong, J. Lu, S. Yao, J. Li, J. Li, Z. Zhong and W. Lu, Application of LIBS for direct determination of volatile matter content in coal, *J. Anal. At. Spectrom.*, 2011, **26**, 2183–2188.
15 A. Matsumoto, A. Tamura, R. Koda, K. Fukami, Y. H. Ogata, N. Nishi and T. Sakka, On-site quantitative elemental analysis of metal ions in aqueous solutions by underwater laser-induced breakdown spectroscopy combined with electrodeposition under controlled potential, *Anal. Chem.*, 2015, **87**, 1655–1661.
16 Y. Chen, M. Dong, J. Cai, H. Chen, Z. Shang and J. Lu, An image auxiliary method for laser-induced breakdown spectroscopy analysis of coal particle flow, *J. Anal. At. Spectrom.*, 2022, **37**, 1126–1133.
17 U. Panne, C. Haisch, M. Clara and R. Niessner, Analysis of glass and glass melts during the vitrification process of fly and bottom ashes by laser-induced plasma spectroscopy. Part I: normalization and plasma diagnostics, *Spectrochim. Acta, Part B*, 1998, **53**, 1957–1968.
18 W. Yin, L. Zhang, L. Dong, W. Ma and S. Jia, Design of a Laser-Induced Breakdown Spectroscopy System for On-Line Quality Analysis of Pulverized Coal in Power Plants, *Appl. Spectrosc.*, 2009, **63**, 865–872.
19 K. Zhan, J. Chen, C. He, Z. Tang, Q. Li, K. Liu, C. Zhu and X. Li, Study on the spectral characteristics and analytical performance of pulverized coal using laser-induced breakdown spectroscopy under a fast physical constraint, *J. Anal. At. Spectrom.*, 2021, **36**, 1210–1216.
20 S. Yao, J. Xu, X. Dong, B. Zhang, J. Zheng and J. Lu, Optimization of laser-induced breakdown spectroscopy for coal powder analysis with different particle flow diameters, *Spectrochim. Acta, Part B*, 2015, **110**, 146–150.
21 Z. Yu, S. Yao, L. Zhang, Z. Lu, Z. S. Lie and J. Lu, Surface-enhanced laser-induced breakdown spectroscopy utilizing metallic target for direct analysis of particle flow, *J. Anal. At. Spectrom.*, 2019, **34**, 172–179.
22 S. Yao, Z. Yu, S. Xu, X. Yao, H. Qin, Z. Lu and J. Lu, Repeatability improvement in laser induced plasma emission of particle flow by aberration-diminished focusing, *Spectrochim. Acta, Part B*, 2021, **175**, 106014.
23 R. Liu, Y. Deguchi, W. Nan, R. Hu, Z. Wang, Y. Fujita, S. Tanaka, K. Tainaka, K. Tanno, H. Watanabe, J. Liu and J. Yan, Unburned carbon measurement in fly ash using laser-induced breakdown spectroscopy with short nanosecond pulse width laser, *Adv. Powder Technol.*, 2019, **30**, 1210–1218.
24 X. Li, Z. Wang, X. Mao and R. E. Russo, Spatially and temporally resolved spectral emission of laser-induced plasmas confined by cylindrical cavities, *J. Anal. At. Spectrom.*, 2014, **29**, 2127–2135.
25 A. M. Popov, F. Colao and R. Fantoni, Spatial confinement of laser-induced plasma to enhance LIBS sensitivity for trace elements determination in soils, *J. Anal. At. Spectrom.*, 2010, **25**, 837–848.
26 H. Yin, Z. Hou, T. Yuan, Z. Wang, W. Ni and Z. Li, Application of spatial confinement for gas analysis using laser-induced breakdown spectroscopy to improve signal stability, *J. Anal. At. Spectrom.*, 2015, **30**, 922–928.
27 L. B. Guo, B. Y. Zhang, X. N. He, C. M. Li, Y. S. Zhou, T. Wu and Y. F. Lu, Optimally enhanced optical emission in laser-induced breakdown spectroscopy by combining spatial confinement and dual-pulse irradiation, *Opt. Express*, 2012, **20**, 1436–1443.
28 L. B. Guo, W. Hu, B. Y. Zhang, X. N. He, C. M. Li, Y. S. Zhou and Y. F. Lu, Enhancement of optical emission from laser-induced plasmas by combined spatial and magnetic confinement, *Opt. Express*, 2011, **19**, 14067–14075.
29 S. Zhao, X. Gao, A. Chen and J. Lin, Effect of spatial confinement on Pb measurements in soil by femtosecond laser-induced breakdown spectroscopy, *Appl. Phys. B*, 2020, **126**, 1–6.
30 X. Bai, Q. Ma, M. Perrier, V. Motto-Ros, D. Sabourdy, L. Nguyen and A. Jalocha, Experimental study of laser-induced plasma: influence of laser fluence and pulse duration, *Spectrochim. Acta, Part B*, 2013, **87**, 27–35.
31 M. Boueri, M. Baudelet, J. Yu, X. Mao, S. S. Mao and R. Russo, Early stage expansion and time-resolved spectral emission of laser-induced plasma from polymer, *Appl. Surf. Sci.*, 2009, **255**, 9566–9571.
32 Y. B. Zel'Dovich and Y. P. Raizer, *Physics of Shock Waves and High-Temperature Hydrodynamic Phenomena*, Dover Publications, Mineola, New York, 2002.
33 T. Li, S. Sahar, Z. Hou, D. Jian and Z. Wang, Impacts of a collection system on laser-induced breakdown spectroscopy signal detection, *Appl. Opt.*, 2018, **57**, 6120–6127.
34 P. Liu, P. J. Ziemann, D. B. Kittelson and P. H. McMurry, Generating particle beams of controlled dimensions and divergence: I. Theory of particle motion in aerodynamic lenses and nozzle expansions, *Aerosol Sci. Technol.*, 1995, **22**, 293–313.
35 J. Dai and J. R. Grace, Blockage of constrictions by particles in fluid–solid transport, *Int. J. Multiphase Flow*, 2010, **36**, 78–87.